



OPEN

DATA DESCRIPTOR

# A Database of Underwater Radiated Noise from Small Vessels in the Coastal Area

Mark Shipton<sup>1,5</sup>, Juraj Obradović<sup>2,5</sup>, Fausto Ferreira<sup>1,2</sup>, Nikola Mišković<sup>2,3</sup>, Tomislav Bulat<sup>4</sup>, Neven Cukrov<sup>4</sup> & Roeë Diamant<sup>1,2</sup>✉

The current procedures for measuring underwater radiated noise (URN) are designed for cooperating vessels in controlled areas. As such, not a lot of data is available for the URN of unidentified vessels of opportunity (VOO), especially for small vessels that do not carry an automatic identification systems (AIS). To this end, we assembled a database of 1148 VOO's URN from acoustic and visual recordings of ferries, fishing boats, yachts, and small speed boats made within Šibenik canal, Croatia. The database comprises source pressure levels at the closest point of approach, picture and video of the vessel, and the vessel's speed, size, and type. A shared webpage allows filtering and comparing vessel types and characteristics. In this paper, we share the structure of our database, the analysis methodology. We conclude that the URN of small vessels is significant and compatible to large vessels.

## Background & Summary

Underwater radiated noise (URN) from shipping activity has been identified as a significant component of ocean ambient noise<sup>1-3</sup>, with recent studies indicating that URN doubles in intensity every decade. The effects of URN on various components of the marine ecosystem, from mussels to marine mammals, have been extensively studied across disciplines<sup>4</sup>. Several reports (e.g.<sup>5,6</sup>) suggest that blunt tissue trauma comparable to blast injuries and behavioral changes reflected in social stability and foraging ability have the potential to affect aquatic animals residing in close proximity to a vessel emitting high sound intensities from its propellers or onboard engines. Research has shown that URN from vessel activity leads to a myriad of adverse effects on fish, crustaceans, and especially on cetaceans<sup>4,7-10</sup>. In particular, the responses of a given aquatic animal to anthropogenic noise can be divided into five main categories<sup>11</sup>: (I) audibility; (II) behavioral responses reflected in changes in the intensity, frequency and intervals of the animal's vocalizations as well as stress behavior; (III) masking of sounds required for communication, localization and foraging; (IV) physiological auditory threshold shifts due to inner ear hair cell fatigue; and (V) physical damage (injury) to the auditory system. In addition, there are direct risks associated with physical disturbance, as in the cases where sea turtles<sup>12</sup> and large baleen whales<sup>13</sup> colliding with vessels, partly because the low-frequency sounds from ships interfere with their navigation. Because of these effects, URNs generated by ships are considered a source of pollution and should be monitored regularly by measuring ship noise.

Shipping URN includes high-power impulsive transient waves generated during ignition<sup>14</sup>, narrow-band noises generated from thrusters, engines as well pumps and generators<sup>15</sup>, and cavitation noises. The latter is caused by the fast enough turn of the propeller to allow low-pressure areas of the propeller to drop below the vapor pressure and the seawater to *boil* at ambient temperature. When the bubbles reach ambient pressure behind the propeller, they implode, yielding broadband stationary noise. The results are: (1) low-frequency noise (around 50 Hz, distributed over a huge area, which impacts the communication of large marine mammals like baleen whales and dolphins); (2) noise from 4-stroke engines (around 200-800 Hz, independent of speed, medium distribution, which likely impacts toothed whales); and (3) high-frequency noise with higher

<sup>1</sup>University of Haifa, Department of Marine Technology, Haifa, 3498838, Israel. <sup>2</sup>University of Zagreb, Faculty of Electrical Engineering and Computing, Zagreb, Unska 3, Croatia. <sup>3</sup>CoE MARBLE - Centre of Excellence in Maritime Robotics and Technologies for Sustainable Blue Economy, Zagreb, Croatia. <sup>4</sup>Division for marine and environmental research, Ruder Bošković Institute, Zagreb, 10000, Croatia. <sup>5</sup>These authors contributed equally: Mark Shipton, Juraj Obradović. ✉e-mail: [roeë.d@univ.haifa.ac.il](mailto:roeë.d@univ.haifa.ac.il)

harmonics due to the Lloyd's mirror effect<sup>16</sup> (1 kHz–10 kHz, speed-dependent, which can bear a significant amount of acoustic energy, and likely effects small mammals and fish).

Standards have been established to limit the transmitted acoustic power per exposure time<sup>17</sup>, and regulatory organizations such as the European Union, the Convention on the Conservation of Migratory Species (CMS), and the Convention on Biological Diversity (CBD), have adopted resolutions aimed at reducing underwater noise from ships and other man-made noise sources. There have even been recent efforts by the shipping industry to reduce URN by creating specialized notations for ships that meet certain noise criteria (e.g., <https://www.lr.org/en/knowledge/press-room/press-listing/press-release/lr-announces-new-underwater-noise-notation/>). Although there are standards for quantifying the URN of vessels<sup>18</sup>, these require the cooperation of the ship: sailing on a fixed route and at nominal speed. The measurement is carried out at deep sea and under low-noise conditions. These conditions do not apply to the URN measurement of a vessel of opportunity (VOO). Specifically, vessels that are not obliged or avoid carrying an automatic identification system (AIS). As a result, the magnitude of noise from such vessels remains under-explored, and a quantitative study examining the extent of shipping URN has yet to be thoroughly conducted. The main barrier to such studies is the establishment of a proper approach to match the size and type of a vessel to its URN.

In this paper, we have addressed the challenge of quantifying the URN of VOO by integrating acoustic measurements with video footage processed using machine learning to estimate the vessel's type, speed, and size. This negated the need to detect the vessel's URN in the acoustic data, and the closest point of access (CPA) could be readily analyzed by time synchronization of the optical and acoustic data. The results of our work is an openly shared dictionary for URN of VOO. The data was collected at the entrance to St. Anthony's Channel near Šibenik, Croatia. Through this channel, a daily traffic of hundreds of vessels exists. Most of these vessels do not carry an AIS but are easy to observe visually as they enter or exit the channel. In total, 1148 vessels were assessed over a period of 23 days. The measured radiated noise took place right below the vessel, where sound propagation is not affected by seasonal changes. Hence, we argue that the period sampled is representable. Our data comprises pictures and videos of the vessels, the spectrum of their URN at the CPA, and meta-data in the form of the vessel's type, size, height, and speed. In the following, we outline our data collection method, the details of the database and its front-end tool that allows comparison of shipping URN.

**Current Approaches in Shipping Noise Measurement.** The literature regarding URN measurement focuses on assessing the noise levels and spectral characteristics of various vessel types under different operating conditions (e.g., speed, cargo load, draft, length, and machinery load). There are currently two main approaches for assessing URN from vessels; the first is a “full-control” approach where specific vessels are chartered to conduct measurements under specified operating conditions<sup>19–21</sup>. This approach requires near full control over the measurement and operating conditions (e.g., speed of the vessel, CPA range), thereby enabling highly accurate measurements as well as the ability to conduct repetitive measurements of the same vessel under different operating conditions. However, the cost-effectiveness of this approach also implies that usually, only a small number of vessels is assessed. The second and more prominent approach is the “opportunistic” or in situ approach, where sensors and data collecting units are placed near main waterways, and measurements of VOOs are acquired as they transit the area<sup>22–24</sup>. While the in situ approach lacks the ability to control the measurement or operating conditions, it does enable the collection of a larger sample number over longer periods of time.

The most common methodology utilized in both the full-control and the in situ approaches is cross-referencing acoustic data collected by hydrophones with vessel data. In this aspect, the introduction of the Automatic Identification System (AIS) in the early 2000s has created an accessible and convenient venue for collecting vessel data. The bulk of current research frameworks have primarily depended on AIS for retrieving vessel data<sup>22,25–27</sup>. While the widespread use of AIS creates more opportunities for full-control and opportunistic URN assessments, it is also important to point out its inherent limitations - as noted in the SOLAS regulation V/19.2 (see <https://www.navcen.uscg.gov/sites/default/files/pdf/AIS/SOLAS.V.19.2.1-5.pdf>), AIS transponders are a legal requirement only for large commercial vessels, e.g., cargo vessels, tankers, passenger ships. This implies that smaller commercial and recreational vessels that are abundant in coastal areas are mostly absent from the current research agenda. The importance of this absence is further emphasized by two aspects. Firstly, the numerical comparison between the number of large commercial vessels and the number of small recreational vessels - the world's total fleet of large commercial vessels is comprised of nearly 109,000 ships (see <https://unctadstat.unctad.org/datacentre/dataviewer/US.MerchantFleet>), while there are nearly 12 million recreational vessels in the US alone<sup>28</sup>. Secondly, the scarce research that has addressed URN from small recreational vessels suggests that under certain conditions, URN from such vessels may be as high or even exceed those of large commercial vessels<sup>25,29,30</sup>. Accordingly, it would seem imperative that a novel approach for assessing URN from smaller vessels is required to fill this gap.

The main challenge for conducting wide-scale assessments of small vessels not equipped with AIS is the retrieval of vessel data in order to collect information on the vessel's type, speed, size, and CPA range. This is available through sensors such as radar and HD cameras. Cope *et al.*<sup>29</sup>, for example, utilized a multi-sensor system (Marine Monitor - M2) comprised of AIS, Radar, and an HD camera for assessing URN levels of vessels. While this approach enables retrieving essential vessel data such as vessel speed, course, and CPA range, other important parameters, such as vessel size, cannot be accurately assessed. To account for the need to collect acoustic data as well as detailed vessel information accurately, we propose a novel approach based on the integration of acoustic and optical sensors.

**Current Approaches in Vessel Detection from Optical Cameras.** The methods for detecting ships using cameras are designed to cope with motion and observation noise. The vessel detection approach in<sup>31</sup> performs background subtraction to detect primary motion in the scene while avoiding interference from wave



**Fig. 1** Setup of the recorder. Left panel: Illustration of the acoustic-optic testbed for quantifying the URN of VOO by using synchronized optical measurements from a shore based camera and an acoustic recorder positioned at the seabed. Right panel: Picture of the underwater acoustic recorder at the deployment site.

motion using saliency detection. Similarly, in<sup>32</sup>, the authors propose a video-based port surveillance that combines context and motion detection. The context part of the algorithm involves graph-based segmentation to identify the ship within the water region, while the motion saliency algorithm utilizes the faster motion of the ship relative to its surroundings. A different approach is proposed in<sup>33</sup>, where eigenvalues of region covariance are computed to distinguish man-made objects from the natural background. Another type of scene separation using optical flow is proposed in<sup>34</sup> to estimate the moving region in the image, and a Gabor filter is implemented for extracting texture features indicating where the ships are located. However, different possible vessel types make it difficult to achieve robust detection and classification.

Due to changing visibility conditions and different shapes of vessels, solutions have recently been developed to identify ships with optical cameras using machine learning methods. These require training with large data sets. For example, the dataset provided in<sup>35</sup> contains 5,500 ship images of 109 different classes taken in the Porto Cesareo Marine Protected Area. Results of ship identification using a discriminatively learned CNN are presented. Another dataset is available in<sup>36</sup>, comprising 70,513 vessels, which were recorded in 48,966 images from 10 camera perspectives. As a basis for vessel identification, the authors propose the Single Shot Detector (SSD) algorithm, which supports significant variations in vessel size and aspect ratios.

Current approaches to vessel identification are based on transfer learning from already trained models. In<sup>37</sup>, the YOLOv3-tiny network is used to recognize vessels and distinguish between six vessel types. For the detection of large vessels, which are easily disturbed by surrounding buildings, waves and lights on the water surface, the Convolutional Block Attention Module (CBAM) is used to focus the model on the target vessel. In<sup>38</sup>, the YOLOv5XL model is used to fuse camera data with AIS information. Through transfer learning, only the last layer was trained with annotated data, which contributes to the generalization of the model. Another application of the YOLOv5 network is presented in<sup>39</sup> to classify between vessel types.

What distinguishes our work from previous work in vessel detection from optical cameras is the use of the YOLOv5 network to detect different types of vessels traveling through narrow canals, and to estimate their size and speed. This system provides more information about the vessel than a bounding box within the image and can manage multiple vessels within a single image. This additional information is used to establish a better link between the vessel's URN and its characteristics and to monitor maritime traffic in narrow areas such as canals, channels, and entrances to marinas with high shipping activity.

## Methods

**Description of the Testbed.** Our testbed resides in the area of St. Anthony's Channel (Sv. Ante in local dialect) Inlet near Šibenik, Croatia. During the summertime, the area is characterized by high-density VOO, which includes various classes of vessels, ranging from coastal commercial ferries to smaller recreational vessels, e.g., yachts, motorboats, and sailboats. Due to the narrow passage, there is only one lane within the channel. These conditions make the area an ideal testbed for analyzing underwater radiated noise from vessels that are not obligated to carry AIS transponders.

The testbed was deployed on August 2023, and aimed to record the URN of VOO passing through the Šibenik channel and to link it with the vessel's size, type and speed. The testbed contained an acoustic recorder and a shore-fixed camera. An illustration of the testbed is shown in Fig. 1.

The acoustic recorder, an AMAR G3 JASCO with a single M36-V35-900 Geospectrum omnidirectional hydrophone, was placed near the eastern entrance to the Channel Inlet at coordinates 43.728400°, 15.879271°. See map in Fig. 2. The hydrophone had a flat with max 0.5 dB ripple response between 0.01-100 kHz and sensitivity of -164.9 dB re:1V/ $\mu$ Pa. At the point of deployment, the channel is 130.3 m wide and most vessels pass in the middle of the channel. The recorder was mounted vertically to an anchor one meter above the seabed at a depth of 29 m. The hydrophone's cage was covered by a dense yellow net to reduce flow noise and assist

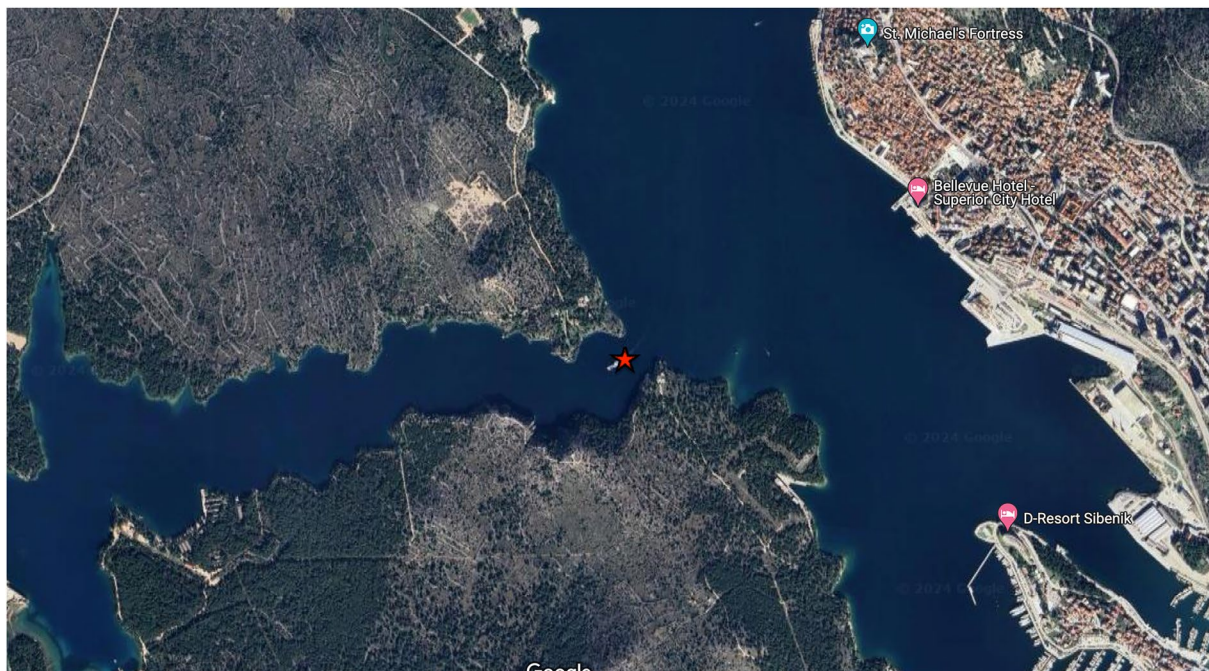


**Fig. 2** A satellite image of the deployment site. The recorder location is marked in red (right next to the vessel in the image).

in locating the recorder after three months of deployment, as shown in Fig. 1. The recorder was set to record continuously for 12 hours a day between 7:00 to 19:00 (UTC+2) to account for daylight hours for the specified region at the time of deployment. The recording was made at a sampling rate of 48 kbps, in a resolution of 3 Bytes per sample. In total, 661 GB were recorded over a period of 113 consecutive days.

The shore-fixed camera was a DAHUA SD-59230U-HNI video camera with an 30x optical zoom. The camera was mounted on a designated stand roughly 800 meters from the canal entrance at coordinates 43.736305°, 15.876754°. The camera was configured to record ships passing through the canal at a continuous rate of 30 FPS at the resolution of 1920 × 1080 pixels. Its 67.8° field of view (FOV) provided a wide perspective of the canal. The camera, which is equipped with an IR night vision device, recorded data continuously, both day and night. However, during the inspection, it was found that the night vision performance did not meet the required range. Therefore, the night data was excluded from the data set, resulting in a total of 340.5 GB of data being collected over a period of 26 days. The camera data was continuously transmitted over a local network and recorded on a PC with sufficient internal memory. The data recording was monitored to avoid possible malfunctions and to ensure uninterrupted data recording. The recorded data was saved in the DAV file format, a compressed and encrypted video format developed by Dahua. To facilitate access and subsequent processing, the DAV files were converted to the more commonly used MP4 format.

Example image from the camera containing two vessels is shown in Fig. 3. For size estimation, the length and height of two landmarks were measured. These are the cretaceous limestone layer, both visible in Fig. 3.

**Visual Analysis.** To analyze the raw optical data, we develop a machine learning based model for vessel detection, tracking and classification from video footage. The model provides a bounding box around the vessel. The algorithm then estimates the meter/pixel ratio and determines the size of the boat in meters from the width of the bounding box. In turn, the tracking procedure follows the bounding box through consecutive frames to estimate the vessel's velocity.

**Vessel Detection and Classification.** For detection, we used the YOLOv5-based trained model which is a fast training model. The details of this implementation are presented in<sup>40</sup> and are given here in brief for completion. The YOLOv5s model is the second smallest of the YOLOv5 family (see code in <https://github.com/ultralytics/yolov5>). The model includes a backbone based on Darknet53 with Cross Stage Partial (CSP)<sup>41</sup>, namely 2 BottleNeckCSP modules and one Spatial Pyramid Pooling (SPP)<sup>42</sup> block (SPPF) with max pooling (kernel pool size = 5) and a neck based on the Path Aggregation Network (PANet). All convolutional layers used a Sigmoid Linear Unit (SiLU) activation function and batch normalization except the three layers that form the head of the network (Sigmoid function).

The model detects and classifies vessels into 9 classes: sailboat, catamaran, small boat, yacht, big yacht, tour boat, passenger boat, trawler, medium boat. For vessel detection and classification, the model was trained using 2100 manually labeled images, observed in 4 different days, and was validated and tested with 100 and 300 images, respectively, captured on days unrelated to the training dataset. Tuned hyper parameters yielded 100



**Fig. 3** Examples of an image with two vessels obtained from the video camera.

Model	Length [m]	Pixel Width	Average Pix. Width	Coefficient	Err to average
Galeon 640 fly	19.81	0.467, 0.467, 0.47, 0.462	0.466	42.438	0.427
Exess 15	14.63	0.366, 0.355	0.361	40.504	2.361
Lagoon 42	12.8	0.295, 0.301, 0.296	0.298	42.940	-0.0745
Antares 650	6.3	0.145, 0.142, 0.144	0.144	43.667	-0.802
Exess 15	14.63	0.359, 0.360, 0.354	0.358	40.827	2.037
Merry F. 1095	10.5	0.248, 0.242	0.245	42.711	0.153
Mali princ	20	0.659, 0.648	0.653	30.585	12.280
Aloha yacht	32.56	0.736	0.736	44.1803	-1.314
Marex 375	12.05	0.280, 0.275, 0.255	0.270	44.549	-1.683
Greenline 40	12.0	0.280, 0.265	0.272	43.969	-1.104
<b>Average coefficient</b>				42.8655	
<b>Standard deviation</b>				1.3485	

**Table 1.** Boat Dimensions and Pixel Coefficients.

epochs and a batch size of 8. Challenges occur in edge cases when a boat exits the frame, causing the bounding box to start shrinking. Avoiding this, we define a region of interest (ROI) that isolates edge positions.

**Vessel Size Estimation.** To determine the meter/pixel conversion rates, we used as ground truth 10 vessels from the collected visual data for which the size is known by factory specifications. This small dataset included speedboats, catamarans and tourist boats for which the size can be easily found online. For each boat, up to 3 images were identified showing the vessel in the beginning, middle, and end of the frame. The meter/pixel ratio was calculated for each of the 10 vessels as the relation between real vessel length and detection bounding box width. A list of all occurrences for the explored 10 vessels is given in Table 1, and examples of the used frames are given in the Fig. 4.

**Velocity estimation.** For estimating the vessel's speed, we applied the SORT (Simple Online and Realtime Tracking) approach<sup>43</sup>, which is based on Kalman filtering. For vessel dynamics, we consider a constant velocity model. We choose SORT due to its ability to maintain track albeit looses of detection for a few frames. This is a typical scenario in our database due to occlusion events where vessels cross each other entering or existing the

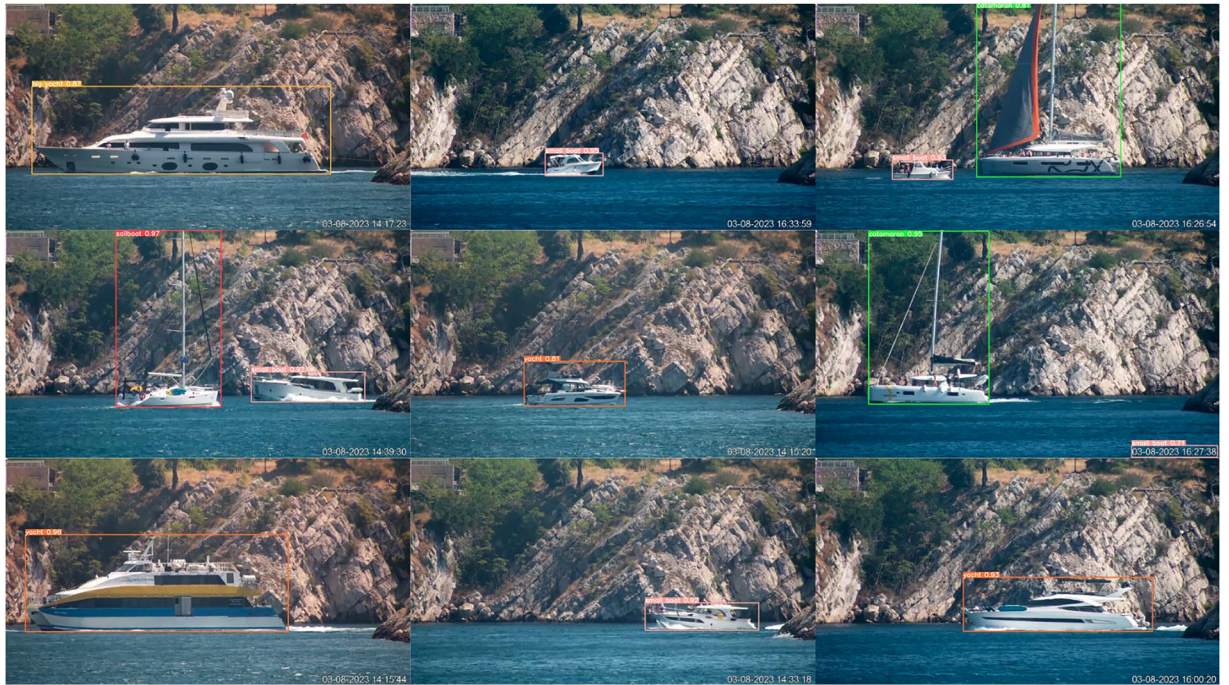


**Fig. 4** Image detections of the boats used for the estimation of meter/pixel coefficient.

canal. The speed of the vessel is calculated by the distance between the bounding boxes at consecutive frames, while accounting for the estimated pixel/meter ratio.

**Vessel Noise Estimation. Quality Control.** To ensure proper synchronization between the acoustic recorder and HD camera throughout the data collection period, the system was subjected to a test trial to check for any time drifts. The internal clocks of the acoustic recorder and HD camera were also compared before and after the data collection period.

Acoustic recording of vessel transits were subjected to quality control on three levels: (1) cross-referencing the data with the HD camera, (2) manually reviewing acoustic samples by an expert analyst, and (3) monitoring real-time weather information. Samples were discarded from the post-analysis under the following criteria.

1. A vessel transit occurred between recording segments;
2. Transit occurred in a time frame where wind speed or sea state exceeded ANSI and ISO standards;
3. If a vessel was employing an active acoustic system (e.g., echo-sounder/Fish-Finder);
4. If a vessel abruptly changed its course or speed;
5. If a vessel conducted a north/south transit and did not enter or exit the channel;
6. If another vessel transited the area within the same time frame;
7. If a marine fauna noise was detected during the vessel's transit.

To calculate the vessel's source level, SL, we reverse-propagate the received acoustic signal, accounting for the transmission loss, TL, to an idealized monopole @ 1m from the source according to ISO standards<sup>44</sup>, such that

$$SL = SPL + TL \quad (1)$$





























This requires the calculation of the SPL and the transmission loss as follows.

**Received Noise Levels.** Received noise levels (RL) measurements were conducted for the full spectrum of 0.023–24 kHz. The upper-frequency limit is set by the sampling rate, while the lower limit accounts for the cutoff frequency resulting from the water depth according to Jensen *et al.*<sup>45</sup>,

$$f_0 = \frac{c}{4D\sqrt{1 - (c/c_b)^2}}, \quad (2)$$

where  $c$  is the sound speed in water,  $c_b$  is the sound speed in the seabed, and  $D$  is the water depth.

The time window length used for URN evaluation, which is an essential aspect of the measurement, varies across different research frameworks. The approach applied in Pine *et al.*<sup>46</sup> and Zhang *et al.*<sup>26</sup>, for instance, utilized a constant time window length with no dependence on the length, speed, or range of the vessel. Other approaches chose to apply a variable time window depending on the vessel's physical characteristics. For

 Name	 Name	 Name
 20230802_105948		 20230803_105552
 20230803_105552		 20230803_105552.mp4
 20230808_104715		 20230803_115552
 20230816_113432		 20230803_115552.mp4
 20230821_100701		 20230803_125552
 20230824_110741		 20230803_125552 .mp4
 20230828_094344		 20230803_135552
 20230830_070413		 20230803_135552 .mp4
 20230904_090103		 20230803_145552
 20230905_113352		 20230803_145552.mp4
 20230906_082812		 20230803_155552
 20230907_082036		 20230803_155552.mp4

**Fig. 5** Organisation of the visual data.

example, in Bahtiarian *et al.*<sup>47</sup> and McKenna *et al.*<sup>22</sup>, the selected time window was dependent on the time it takes for a vessel to travel its length. Unfortunately, neither of these options is suitable for our setup. In particular, as the results in Figs. 6, 7 show, our database includes significant variances in vessel transit speeds and lengths. Instead, we chose to follow the ISO<sup>44</sup> standard, which sets a variable time window dependent on the aspect of each vessel (60–120 deg of the bow aspect). Here, the time window length was calculated based on the vessel's speed, as reported by the visual algorithm.

To measure the SPL, we applied (3); the variable time window used for the measurement of each vessel transit was processed in the frequency domain by a fast-Fourier transform (2048 FFT points, Hanning window with a 50% overlap). The 2048 FFT resolution was chosen to allow comparability with other research frameworks<sup>48,49</sup>.

$$\text{SPL} = 20 \log_{10} \left( \frac{P_{\text{RMS}}}{P_{\text{ref}}} \right), \quad (3)$$

where  $P_{\text{ref}} = 1 \mu\text{Pa}$  and  $P_{\text{RMS}}$  is the root mean square of the sound pressure level measured within the variable time window. For the measurement of third-octave bands, we applied the same parameters, albeit with a higher frequency resolution (32,768 FFT points), in order to comply with standard one-third octave bands according to the ANSI Standard S1.11-2014/Part 1<sup>50</sup>.

**Transmission Loss.** The acoustic transmission loss depends on the range of the vessel, geometric spreading characteristics, and the seabed and water column properties<sup>51</sup>. Referring to the vessel's range, while the entrance to the inlet is measured at 135.7 m, our observations showed that nearly all marine traffic passes through a ~90 m lateral area in the middle of the channel inlet. These observations coincide with known hazards to safe navigation and official maritime routes described in maritime charts. Based on this information, we calculate the maximum potential CPA range as the slant between the hydrophone and the described lateral area (49 m) and the minimum potential CPA range as 29 m (water depth to hydrophone). For the geometric transmission loss calculations, we applied the mean CPA range (39 m). This  $\pm 10$  m ambiguity in the vessel's location can be compared with the location error of URN databases relying on AIS information, which is known to present a mean discrepancy of up to 97.72 m<sup>52</sup>.

In the aspect of absorption losses, applying Ainslie and McCole's<sup>53</sup> equation for absorption in seawater for the mean CPA range under different scenarios of temperature and salinity found in the tested area, we reach a

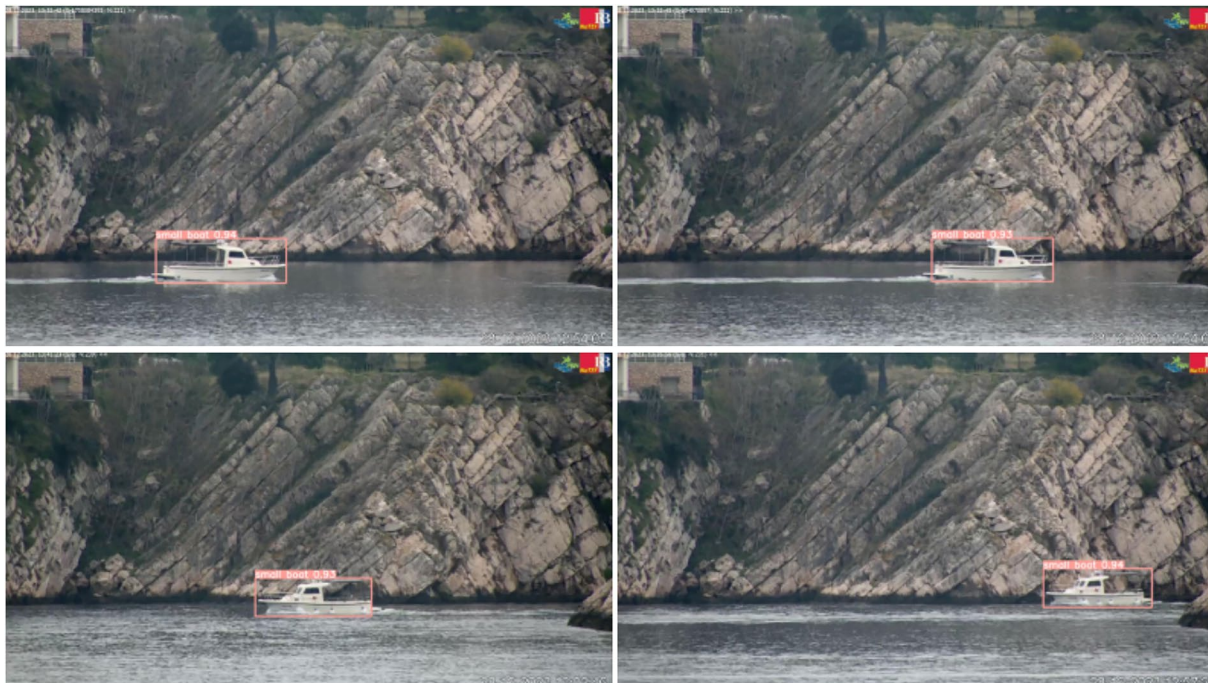


**Fig. 6** Histogram of vessel classes the final vessel detection result.

maximum loss of roughly 0.15 dB at the mean CPA range. We, therefore, consider absorption losses as negligible. Similar conclusions about the negligibility of absorption losses in URN levels of vessels at close ranges have been made in Hermann *et al.*<sup>54</sup> and McKenna *et al.*<sup>22</sup>. As the type of sediment in the test bed area consists primarily of fine gravel<sup>55</sup>, which possesses a high reflective coefficient<sup>21</sup>, we chose to apply the simplified equation described by Erbe<sup>56</sup>, which has also been used in similar research frameworks<sup>57</sup>,

$$TL = 20\log_{10}(D) + 10\log_{10}(R/D), \quad (4)$$

where  $R$  is the horizontal range between the mean CPA and the receiver and we recall that  $D$  is the water depth.

### Data Records

The repository data is at Science Data Bank<sup>58</sup>. We declare that the openly sharing of all videos, images and acoustic recordings of the ships in our dataset are in compliance with all ethical and legal considerations. We declare all approvals and permissions required for the open publication of the data have been granted. In particular, institute Ruder Boskovic, as a state scientific institution, has the permission to perform research on the territory of the Republic of Croatia. A permit for research in the protected area of Krka estuary, where the data was collected, has been obtained. This permit was given since 2014 as part of the project “Nautical Tourism Ecological Footprint in MPAs” financed by MEDPAN, to log data and provide local authorities with information about vessels passing through.

In this section we describe the arrangement of the data.

**Arrangement of Data files.** *Visual Information.* The optical dataset is organized into 12 folders, each named according to the starting time of the recording in the format `yyyymmdd_hhmmss`. Each folder contains pairs of 1-hour video files and corresponding `.csv` files. In total, there are 324 `.csv` files. Each `.csv` file contains detection information with the following columns:

- `time_of_detection`: The time at which the detection occurred.
- `boat_class`: The class of the detected boat.
- `size`: The size of the detected boat.
- `velocity`: The velocity of the detected boat.

An example for the visual data architecture is shown in Fig. 5.

*Acoustic Information and Online Database.* The acoustic dataset and processed acoustic information include the time and date of transit, the type of vessel, the sub-type of the vessel, the length and speed of the vessel (according to the visual algorithm), the calculated SL–SPL, and one-third octave spectrogram, and, where applicable, the full name and IMO number.



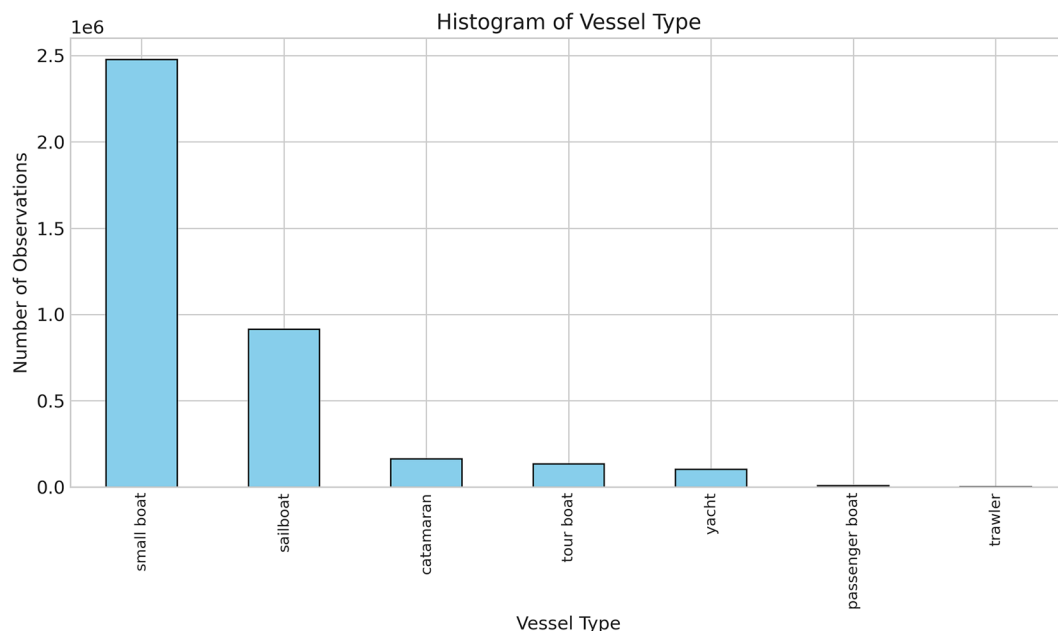


**Fig. 7** Histogram of vessels size in the final vessel detection result.

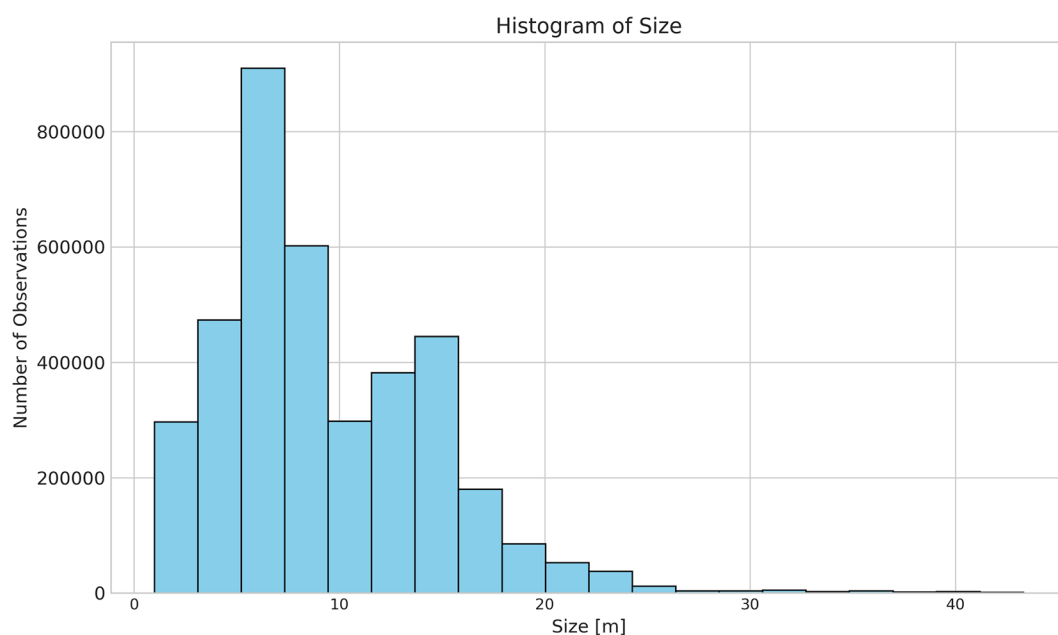


**Fig. 8** Histogram of vessels velocity in the final vessel detection result. Positive speed reflects vessels exiting the channel, and vice versa for vessels entering the channel.

### Technical Validation

**Vessel Detection Results by Optical Camera.** *Summary of Detected Vessels.* Our dataset contains 3,799,505 camera detections of various types of vessels, along with their corresponding detection times, estimated sizes, and velocities. The histogram in Fig. 6 indicates that the “small boat” class is by far the most common in this dataset, representing around 65% of all detected vessels. Additionally, sailboats are frequently observed, likely due to the presence of charter marinas in the area. A distribution of vessel sizes is presented in Fig. 7. The data reveals maxima at around 5–8 meters, which is a common size for vessels classified as small boats, and at 12–15 meters, which is typical for regular sailboats.

The histogram in Fig. 8 shows the density of vessels’ velocities. We determine positive speed for vessels exiting the channel towards the port and vice versa for vessels entering the channel. Results show that vessels moving towards the port move slower compared to those heading towards open sea. Most vessels travel at an absolute speeds of  $2.5\text{--}4.0\text{ ms}^{-1}$  (4.85–7.7 knots). This is expected, considering that the most frequently detected class was small boats.

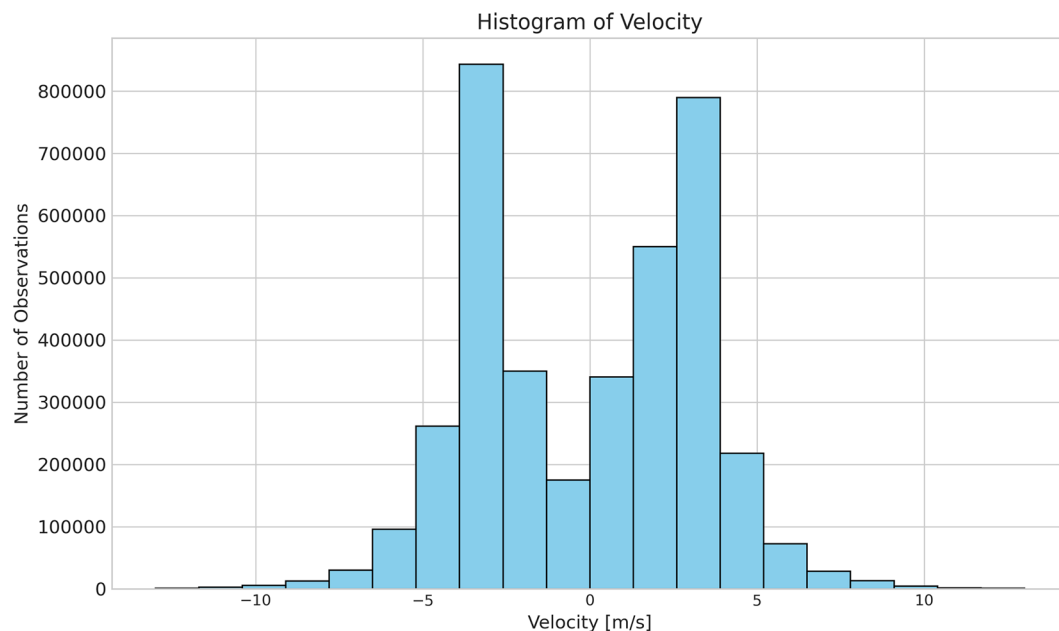


**Fig. 9** Detections on the vessel with known size for the purpose of algorithm performance evaluation.

**Results of Vessel Size and Speed Estimations.** To examine the algorithm's performance in estimating vessel size and velocity, a small dataset was created with the vessels of known size and speed. The picture in Fig. 9 is of a small research vessel belonging to the Institute Ruđer Bošković, with a measured waterline length of 8 m and a total length of 9.3 m. To evaluate the size estimation error, the boat performed two transactions on both the left and right sides of the channel. The images collected from 4 such passages are shown in Fig. 9.

Successful detection and classification occur in all frames. However, due to the angle of the vessel, the final part of the stern is included in the bounding box of only some of the frames. Size estimation results of the test vessel for 6 corresponding frames are given in Table 2. The average length of 8.495 m is close to the waterline length, and a standard deviation of 0.2187 m represents roughly 3% of the average value. We deem this error acceptable considering the use of a single monocular camera.

Another validation of the size and velocity measurements was performed over incidences involving vessels carrying AIS. To this end, we filtered a large dataset of 65,000 AIS recorded at a low frame rate of 5 min within the channel. That resulted in only 9 recordings that aligned with the camera frame allowing us to match the AIS data with the camera data accurately. This low number of vessels emphasizes the low rate of detection available for shipping URN measurements using AIS data only. The true and estimated size and speed of these 9 vessels are listed in Table 3. An average error of roughly 7% in both length and speed is observed. Part of this error is due to the rounding operation of the AIS.

**Results of Shipping Noise Estimation.** Of the thousands of vessel transits recorded by the visual algorithm, 1148 passed quality control (see Quality Control Section) and were processed to extract their acoustic characteristics, i.e., sound pressure level and 1/3 octave spectrum. Each vessel transit was labeled according to its type, the time and date of the transit, as well as the vessel hull name and IMO number, where applicable. The hull name and IMO no. were associated to a vessel transit in cases where the hull name was visible via the camera footage. The length and speed of each transit were associated according to the calculations made by the visual algorithm. Table 4 presents an overview of the analyzed vessels' characteristics, i.e., class, number of observations, speed, length, and the calculated sound pressure levels at the source (SL-SPL). The largest vessel observed in the dataset was a 54-meter mega-yacht named "Premier" (IMO 9949132), while the smallest is a 3.3-meter motorboat. The fastest vessel analyzed is a motorboat sailing at 15.9 meters per second (m/sec), i.e., 31 knots. The slowest vessel is a sailboat sailing at 1.1 m/sec. The loudest vessel observed was the *Postira* ferry (IMO 6283202) sailing at 6.5 m/sec, which presented a calculated source level of 188.26 dB, and the quietest vessel was a sailboat sailing at 2.4 m/sec which presented a calculated source level of 151.91 dB.

### Usage Notes

In addition to the dataset file, the data is available at a front end called "Hear my ship" (<https://hearmyship.fer.hr/>). The web tool allows separation by vessel's type, speed, length and noise, visualization of the data (both optics and acoustics), data download and comparison between the URNs of different vessels.

Overall, 1148 vessel transits were evaluated. As mentioned in the introduction Section, URN calculations for small vessels in the coastal area have been mostly absent from the current research agenda, primarily due to the lack of any open-source information systems that broadcast vessel data (e.g., AIS found on larger commercial vessels). This, in turn, creates inherent difficulties in collecting vessel parameters, e.g., length and speed, which are crucial parameters for URN calculations. In this sense, the novel methodology implemented in this research

Video Frame	Bounding Box	Estimated Length
1	(0.357, 0.745, 0.214, 0.130)	9.15 m
2	(0.622, 0.743, 0.199, 0.126)	8.53 m
3	(0.794, 0.697, 0.178, 0.113)	7.64 m
4	(0.357, 0.745, 0.214, 0.130)	9.15 m
5	(0.611, 0.727, 0.194, 0.111)	8.33 m
6	(0.508, 0.724, 0.191, 0.111)	8.17 m
<b>Average Length</b>	8.495 m	
<b>Standard Deviation</b>	0.2187 m	

**Table 2.** Test results for the Ruđer Bošković Research Vessel (waterline length of 8 m and total length of 9.3 m).

Boat Index	Length [m]	Estimated Length [m]	Velocity [ $\text{ms}^{-1}$ ]	Estimated Velocity [ $\text{ms}^{-1}$ ]
1	12.0	14.48696	6.1	6.99
2	12.0	12.97377	5.1	4.47
3	15.0	16.89319	6.4	6.61
4	15.0	15.37999	5.6	5.25
5	14.0	14.2389	5.0	5.25
6	14.0	14.53657	5.0	5.05
7	17.0	19.39864	6.2	5.44
8	17.0	18.65444	6.4	5.83
9	13.0	13.34587	5.2	5.05
<b>Average error</b>	7.707%		7.395%	
<b>Error Std. Dev</b>	5.368%		4.855%	

**Table 3.** Test results for length and speed estimations for 9 vessels identified by both camera and AIS.

Class	Number of Observations	Speed [m/sec]	Length [m]	SL-SPL [dB]
<b>Ferry</b>	50	5.66 / 0.63	41.95 / 6.43	178.16 / 5.79
<b>Auxiliary Vessel</b>	1	3.5	35.77	176
<b>Cargo Vessel</b>	2	3.1 / 0.28	44	179.45 / 1.916
<b>Fishing Vessel</b>	2	3.60 / 0.28	13.48 / 6.31	167.35 / 0.50
<b>Tour Boat</b>	63	3.44 / 0.61	21.01 / 2.43	167.11 / 4.77
<b>Diving Boat</b>	1	2.80	15.33	172.22
<b>Yacht</b>	124	4.27 / 0.96	25.65 / 10.96	172.12 / 5.64
<b>Sailboat</b>	192	3.22 / 0.63	15.38 / 4.12	162.46 / 5.35
<b>Motor Boat</b>	713	5.15 / 2.00	7.88 / 2.14	170.96 / 4.49
<b>Full Dataset</b>	<b>1148</b>	<b>4.65 / 1.82</b>	<b>13.38 / 9.86</b>	<b>169.79 / 6.12</b>

**Table 4.** Characteristics of the Vessel Dataset (mean / Std. Dev).

framework enabled the formation of what can be considered the most comprehensive dataset to date, specifically focused on small to medium vessels.

In making our database of URN of VOO, our biggest concern was the averaging window around the CPA for URN estimation. The size of this window should be long enough to suppress noise but also short enough to avoid differences in the received power due to the changing distances between the receiver and the moving vessel. In our database, we have followed the method recommended in ISO 17208<sup>44</sup> that manages this trade-off by setting the observation window as the time-frame in which the vessel passes the  $\pm 30^\circ$  aspect tangent to the hydrophone. However, for some of the fast motorboats sailing at  $>10$  m/sec, this resulted in relatively short time-window lengths ( $\sim 4$  s). A possible way to address this challenge is a statistical measure to test the stability of the acoustic intensity around the CPA and to determine the size of the observation time accordingly.

Another challenge encountered is the extensive traffic of vessels within the channel where the recordings took place. To avoid any mutual interference caused by vessels transiting the channel in close proximity, we placed a strict quality control process (see Section below) and dismissed cases identified by the video footage or acoustics of vessels transiting the channel in close proximity. As a result, roughly 90% of the vessel transits did not pass quality control. The case of too close vessels also poses a challenge for monitoring the URN of VOO in realistic conditions of near port measurements.

### Code availability

The code for the optical and acoustic processing performing ship detection, classification, and size, speed estimation, and acoustic statistical calculations are available in the data repository<sup>59</sup>.

Received: 18 September 2024; Accepted: 30 January 2025;

Published online: 18 February 2025

## References

1. Wenz, G. M. Acoustic ambient noise in the ocean: Spectra and sources. *The journal of the acoustical society of America* **34**, 1936–1956 (1962).
2. Hildebrand, J. A. Anthropogenic and natural sources of ambient noise in the ocean. *Marine Ecology Progress Series* **395**, 5–20 (2009).
3. Southall, B. L. *et al.* Underwater noise from large commercial ships-international collaboration for noise reduction. *Encyclopedia of Maritime and Offshore Engineering* 1–9 (2017).
4. Erbe, C. *et al.* The effects of ship noise on marine mammals—a review. *Frontiers in Marine Science* **6**, 476898 (2019).
5. Gordon, J. *et al.* A review of the effects of seismic surveys on marine mammals. *Marine Technology Society Journal* **37**, 16–34 (2003).
6. Nelms, S. E., Piniak, W. E., Weir, C. R. & Godley, B. J. Seismic surveys and marine turtles: An underestimated global threat? *Biological conservation* **193**, 49–65 (2016).
7. Blom, E.-L. *et al.* Continuous but not intermittent noise has a negative impact on mating success in a marine fish with paternal care. *Scientific reports* **9**, 5494 (2019).
8. Buscaino, G. *et al.* Impact of an acoustic stimulus on the motility and blood parameters of european sea bass (*dicentrarchus labrax* L.) and gilthead sea bream (*sparus aurata* L.). *Marine environmental research* **69**, 136–142 (2010).
9. Carter, E. E., Tregenza, T. & Stevens, M. Ship noise inhibits colour change, camouflage, and anti-predator behaviour in shore crabs. *Current Biology* **30**, R211–R212 (2020).
10. Diamant, R., Testolin, A., Shachar, I., Galili, O. & Scheinin, A. Observational study on the non-linear response of dolphins to the presence of vessels. *Scientific Reports* **14**, 6062 (2024).
11. Erbe, C., MacGillivray, A. & Williams, R. Mapping cumulative noise from shipping to inform marine spatial planning. *The Journal of the Acoustical Society of America* **132**, EL423–EL428 (2012).
12. Casale, P. *et al.* Mediterranean sea turtles: current knowledge and priorities for conservation and research. *Endangered species research* **36**, 229–267 (2018).
13. Sèbe, M., Christos, A. K. & Pendleton, L. A decision-making framework to reduce the risk of collisions between ships and whales. *Marine Policy* **109**, 103697 (2019).
14. Jensen, F. H. *et al.* Vessel noise effects on delphinid communication. *Marine Ecology Progress Series* **395**, 161–175 (2009).
15. Arveson, P. T. & Vendittis, D. J. Radiated noise characteristics of a modern cargo ship. *The Journal of the Acoustical Society of America* **107**, 118–129 (2000).
16. Audoly, C. & Meyer, V. Measurement of radiated noise from surface ships-influence of the sea surface reflection coefficient on the lloyd's mirror effect. In *ACOUSTICS 2017* (2017).
17. CMRE. Sonar acoustics handbook by center for maritime research & experimentation (CMRE). In *Animal communication and noise*, 20–23 (UComms 18 special edition, 2018).
18. Gassmann, M., Wiggins, S. M. & Hildebrand, J. A. Deep-water measurements of container ship radiated noise signatures and directionality. *The journal of the acoustical society of America* **142**, 1563–1574 (2017).
19. Zhu, C., Gaggero, T., Makris, N. C. & Raitil, P. Underwater sound characteristics of a ship with controllable pitch propeller. *Journal of Marine Science and Engineering* **10**, 328 (2022).
20. Salio, M. P. Numerical assessment of underwater noise radiated by a cruise ship. *Ships and Offshore Structures* **10**, 308–327 (2015).
21. Grelowska, G., Kozaczka, E., Kozaczka, S. & Szymczak, W. Underwater noise generated by a small ship in the shallow sea. *Archives of Acoustics* **38**, 351–356 (2013).
22. McKenna, M. F., Ross, D., Wiggins, S. M. & Hildebrand, J. A. Underwater radiated noise from modern commercial ships. *The Journal of the Acoustical Society of America* **131**, 92–103 (2012).
23. Allen, J. K., Peterson, M. L., Sharrard, G. V., Wright, D. L. & Todd, S. K. Radiated noise from commercial ships in the gulf of maine: Implications for whale/vessel collisions. *The Journal of the Acoustical Society of America* **132**, EL229–EL235 (2012).
24. Merchant, N. D., Blondel, P., Dakin, D. T. & Dorocicz, J. Averaging underwater noise levels for environmental assessment of shipping. *The Journal of the Acoustical Society of America* **132**, EL343–EL349 (2012).
25. Veirs, S., Veirs, V. & Wood, J. D. Ship noise extends to frequencies used for echolocation by endangered killer whales. *PeerJ* **4**, e1657 (2016).
26. Zhang, G., Forland, T. N., Johnsen, E., Pedersen, G. & Dong, H. Measurements of underwater noise radiated by commercial ships at a cabled ocean observatory. *Marine Pollution Bulletin* **153**, 110948 (2020).
27. ZoBell, V. M. *et al.* Underwater noise mitigation in the santa barbara channel through incentive-based vessel speed reduction. *Scientific reports* **11**, 18391 (2021).
28. USCG. 2022 recreational boating statistics Accessed on 01-07-2024. (2023).
29. Cope, S. *et al.* Multi-sensor integration for an assessment of underwater radiated noise from common vessels in san francisco bay. *The Journal of the Acoustical Society of America* **149**, 2451–2464 (2021).
30. Picciulin, M. *et al.* Characterization of the underwater noise produced by recreational and small fishing boats (<14 m) in the shallow water of the cres-lošinj natura 2000 sci. *Marine pollution bulletin* **183**, 114050 (2022).
31. Tran, T.-H. & Le, T.-L. Vision based boat detection for maritime surveillance. In *2016 International Conference on Electronics, Information, and Communications (ICEIC)*, 1–4 (IEEE, 2016).
32. Bao, X., Zinger, S., Wijnhoven, R. *et al.* Ship detection in port surveillance based on context and motion saliency analysis. In *Video Surveillance and Transportation Imaging Applications*, vol. 8663, 87–94 (SPIE, 2013).
33. Dong, C., Liu, J.-H., Xu, F., Wang, R.-H. *et al.* Fast ship detection in optical remote sensing images. *Journal of Jilin University (Engineering and Technology Edition)* (2019).
34. Li, H. & Man, Y. Moving ship detection based on visual saliency for video satellite. In *2016 IEEE International Geoscience and Remote Sensing Symposium (IGARSS)*, 1248–1250. <https://doi.org/10.1109/IGARSS.2016.7729316> (2016).
35. Spagnolo, P., Filieri, F., Distanto, C., Mazzeo, P. L. & D'Ambrosio, P. A new annotated dataset for boat detection and re-identification. In *2019 16th IEEE International Conference on Advanced Video and Signal Based Surveillance (AVSS)*, 1–7. <https://doi.org/10.1109/AVSS.2019.8909831> (2019).
36. Zwemer, M. H., Wijnhoven, R. G. & de With, P. H. Ship detection in harbour surveillance based on large-scale data and cnns. In *VISIGRAPP (5: VISAPP)*, 153–160 (2018).
37. Li, H., Deng, L., Yang, C., Liu, J. & Gu, Z. Enhanced yolo v3 tiny network for real-time ship detection from visual image. *IEEE Access* **9**, 16692–16706. <https://doi.org/10.1109/ACCESS.2021.3053956> (2021).
38. Lu, Y. *et al.* Fusion of camera-based vessel detection and AIS for maritime surveillance. In *2021 26th International Conference on Automation and Computing (ICAC)*, 1–6 (IEEE, 2021).
39. Gülsoylu, E., Koch, P., Yildiz, M., Constapel, M. & Kelm, A. P. Image and AIS data fusion technique for maritime computer vision applications. In *Proceedings of the IEEE/CVF Winter Conference on Applications of Computer Vision*, 859–868 (2024).
40. Correia, A., Ferreira, F. & Mišković, N. Comparing different yolo versions for boat detection and classification in real datasets. In *OCEANS 2024 Singapore* (IEEE, 2024). Accepted for publication.

41. Wang, C.-Y. *et al.* Cspnet: A new backbone that can enhance learning capability of cnn. In *2020 IEEE/CVF Conference on Computer Vision and Pattern Recognition Workshops (CVPRW)*, 1571–1580, <https://doi.org/10.1109/CVPRW50498.2020.00203> (2020).
42. He, K., Zhang, X., Ren, S. & Sun, J. Spatial pyramid pooling in deep convolutional networks for visual recognition. *IEEE Transactions on Pattern Analysis and Machine Intelligence* **37**, 1904–1916, <https://doi.org/10.1109/TPAMI.2015.2389824> (2015).
43. Bewley, A., Ge, Z., Ott, L., Ramos, F. & Upcroft, B. Simple online and realtime tracking. In *2016 IEEE international conference on image processing (ICIP)*, 3464–3468 (IEEE, 2016).
44. for Standardization, I. O. Iso/dis 17208-3(en) underwater acoustics - quantities and procedures for description and measurement of underwater sound from ships - part 3: Requirements for measurements in shallow water [Accessed 10-06-2024] (2019).
45. Jensen, F. B., Kuperman, W. A., Porter, M. B., Schmidt, H. & Tolstoy, A. *Computational ocean acoustics*, vol. 2011 (Springer, 2011).
46. Pine, M. K., Jeffs, A. G., Wang, D. & Radford, C. A. The potential for vessel noise to mask biologically important sounds within ecologically significant embayments. *Ocean & Coastal Management* **127**, 63–73 (2016).
47. Bahtiarian, M. A. Asa standard goes underwater. *Acoust. Today* **5**, 26–29 (2009).
48. Mahanty, M. M., Latha, G., Raguraman, G., Venkatesan, R. *et al.* Passive acoustic detection of distant ship crossing signal in deep waters using wavelet denoising technique. In *OCEANS 2022-Chennai*, 1–5 (IEEE, 2022).
49. Song, G. *et al.* Underwater noise classification based on support vector machine. In *2021 OES China Ocean Acoustics (COA)*, 410–414 (IEEE, 2021).
50. ANSI. ANSI/ASA S1.11-2014/Part 1 / IEC 61260:1-2014 - Electroacoustics - Octave-band and Fractional-octave-band Filters - Part 1: Specifications (a nationally adopted international standard — webstore.ansi.org [Accessed 10-06-2024] (2014).
51. Marsh, H. & Schulkin, M. *Underwater sound transmission* (Avco Corporation, Marine Electronics Office, 1962).
52. Jankowski, D., Lamm, A. & Hahn, A. Determination of ais position accuracy and evaluation of reconstruction methods for maritime observation data. *IFAC-PapersOnLine* **54**, 97–104 (2021).
53. Ainslie, M. A. & McColm, J. G. A simplified formula for viscous and chemical absorption in sea water. *The Journal of the Acoustical Society of America* **103**, 1671–1672 (1998).
54. Hermannsen, L., Beedholm, K., Tougaard, J. & Madsen, P. T. High frequency components of ship noise in shallow water with a discussion of implications for harbor porpoises (*phocoena phocoena*). *The Journal of the Acoustical Society of America* **136**, 1640–1653 (2014).
55. Huljek, L., Strmić Palinkaš, S., Fiket, Ž. & Fajković, H. Environmental aspects of historical ferromanganese tailings in the šibenik bay, croatia. *Water* **13**, 3123 (2021).
56. Erbe, C. Underwater acoustics: noise and the effects on marine mammals. *A Pocket Handbook* **164**, 10–35 (2011).
57. Sipilä, T., Viitanen, V., Uosukainen, S. & Klose, R. Shallow water effects on ship underwater noise measurements. In *48th International Congress and Exhibition on Noise Control Engineering, INTER-NOISE 2019, 1707* (Institute of Noise Control Engineering, 2019).
58. Obradović, J. & Shipton, M. Raw data for the hearmyship data repository: optical and acoustic files of vessels, <https://doi.org/10.57760/sciencedb.13099> [Accessed 11-09-2024] (2024).
59. Obradović, J. & Shipton, M. Code for the processing of the hearmyship data repository: optical and acoustic, <https://doi.org/10.57760/sciencedb.13532> [Accessed 11-09-2024] (2024).

## Acknowledgements

The authors would like to thank Shlomi Dahan and Mak Gračić for their help in acquiring the acoustic data, and to Matej Radović and Đula Nađ for their help in setting up the web front. This research was supported by a scholarship sponsored by the Israeli Science Foundation (grant #973/23), by the University of Haifa's Innovation & Sustainability Division, and by the Horizon Europe program of the European Union under the UWIN-LABUST project (project #101086340).

## Author contributions

M.S. analyzed the acoustic data, created the database, and wrote the manuscript; J.O. and F.F. analyzed the visual data and wrote the manuscript; N.M. assisted with administration, provided funding, and edited the manuscript; T.B. and N.B. acquired the acoustic and visual data; R.D. supervised the project, acquired the acoustic dataset, provided funding and wrote the manuscript.

## Competing interests

The authors declare no competing interests.

## Additional information

**Correspondence** and requests for materials should be addressed to R.D.

**Reprints and permissions information** is available at [www.nature.com/reprints](http://www.nature.com/reprints).

**Publisher's note** Springer Nature remains neutral with regard to jurisdictional claims in published maps and institutional affiliations.



**Open Access** This article is licensed under a Creative Commons Attribution-NonCommercial-NoDerivatives 4.0 International License, which permits any non-commercial use, sharing, distribution and reproduction in any medium or format, as long as you give appropriate credit to the original author(s) and the source, provide a link to the Creative Commons licence, and indicate if you modified the licensed material. You do not have permission under this licence to share adapted material derived from this article or parts of it. The images or other third party material in this article are included in the article's Creative Commons licence, unless indicated otherwise in a credit line to the material. If material is not included in the article's Creative Commons licence and your intended use is not permitted by statutory regulation or exceeds the permitted use, you will need to obtain permission directly from the copyright holder. To view a copy of this licence, visit <http://creativecommons.org/licenses/by-nc-nd/4.0/>.

© The Author(s) 2025